Computational Materials Science 223 (2023) 112116

Contents lists available at ScienceDirect

Computational Materials Science

journal homepage: www.elsevier.com/locate/commatsci

Full Length Article

Effects of oxidizers on the ignition and combustion characteristics of aluminum nanoparticles

Yintao Zhou [a], Baolu Shi [a], Qingzhao Chu [b,*], Lijuan Liao [c,*]

[a] School of Aerospace Engineering, Beijing Institute of Technology, No. 5 Zhongguancun South Street, Haidian, Beijing 100081, China
[b] State Key Laboratory of Explosion Science and Technology, Beijing Institute of Technology, No. 5 Zhongguancun South Street, Haidian, Beijing 100081, China
[c] Key Laboratory for Mechanics in Fluid Solid Coupling Systems, Institute of Mechanics, Chinese Academy of Sciences, Beijing 100190, China

ARTICLE INFO

Keywords:
Aluminum nanoparticles
Oxidizer atmospheres
Ignition and combustion
Energy release
Reactive molecular dynamic simulation

ABSTRACT

Ignition and combustion of Aluminum nanoparticles (ANPs) under complex environments are of great significance for various propulsion systems. In this study, we investigated the oxidation process of ANPs in O_2, CO_2, H_2O, and their mixture atmospheres using reactive molecular dynamics. In the mixture atmospheres, ANPs experience a shorter ignition delay and parts of C and H atoms are involved in a new reaction named re-oxidation, where the nonbonded C and H inside ANPs detach from particle and re-bond with free O in the environment to produce extra CO and H_2O. It reduces C and H in unreactive diffusion and increases O in reactive diffusion. Additionally, it is found that the ignition delay time and reaction heat release can be adjusted to achieve the optimal performance of ANPs combustion by tailoring the contents of O_2, CO_2, and H_2O in the environment. Our works provide a theoretical basis for the precise regulation of ANPs energy release.

1. Introduction

Aluminum particles, owing to their high enthalpy, high specific energy density [1], and non-toxic products [2], have been widely used in a variety of propulsion systems [3–6]. The difficulty of ignition and combustion of aluminum microparticles [7] brings great challenges to their practical application. Therefore, Aluminum nanoparticles (ANPs) have attracted more and more attention for their remarkable performances, such as high specific surface area, low ignition temperature, and high reaction rate [8].

In recent decades, a lot of researches have been conducted on the reaction mechanism of ANPs, and the effects of alumina shell structures [9], diffusion rate of aluminum and oxygen atoms [10], particle size [11], phase transition [12], shell melting and core reacting [13], and environmental temperature and pressure [14,15] have been analyzed by experiments and simulations. Besides, the oxidizer property in the atmosphere is also a significant factor in the ignition and combustion process of ANPs. Oxygen is the most important oxidizer for ANPs combustion and has been extensively studied. Rai et al. [16] established the diffusion combustion model of ANPs in O_2. They argued that oxygen diffused from the outer surface of the particle to the reaction surface during combustion, while aluminum diffused from the core/shell interface to the reaction surface. Based on the direct simulation Monte Carlo (DSMC) and CFD simulations, Zou et al. [17] proposed a theoretical model to describe the ignition characteristics of aluminum particles burning in the O_2 atmosphere. Two formulas were obtained to predict the ignition temperature and ignition delay time for nano/microparticles. Zhang et al. [18] employed molecular dynamics simulations to explore the oxidation process of ANPs with a diameter of 5 nm under different oxygen concentrations. They observed that the oxidized ANPs would form three morphological structures as the oxygen content increased: core–shell structure, core-chain structure, and oxide cluster. Li et al. [19] found that when ANP was burning in a high-temperature, high-density O_2 atmosphere, a micro-explosion phenomenon occurred, accelerating the oxidation process. Experimental results of Tang et al. [20] also proved that ANP would experience mild oxidation to micro-explosion with the increasement of O_2 concentration.

However, in practical applications, ANPs often burn in an oxygen-deprived environment. During Mars exploration, CO_2 is the primary oxidant to provide energy for the propulsion system [21]. In addition, the reaction between ANP and H_2O is also a technical means of making hydrogen, a potential energy source [22,23]. Therefore, the reaction between ANP and CO_2/H_2O has gradually received researchers' interest. Chu et al. [24] simulated the burning of ANPs in three typical oxidizers (O_2, CO_2, and H_2O). They revealed three modes of ANP oxidation, including physical and chemical adsorption on the surface and

* Corresponding authors.

https://doi.org/10.1016/j.commatsci.2023.112116
Received 9 December 2022; Received in revised form 28 February 2023; Accepted 2 March 2023
Available online 15 March 2023

Table 1
Information on six system settings.

System	N_{O2}	N_{CO2}	N_{H2O}
ANP-O_2	2700	0	0
ANP-CO_2	0	2700	0
ANP-H_2O	0	0	2700
ANP-O_2 + CO_2	1350	1350	0
ANP-O_2 + H_2O	1350	0	1350
ANP-O_2 + CO_2 + H_2O	900	900	900

subsequent reactive diffusion inside the ANP. Meanwhile, They also observed that the reaction between ANP and CO_2 would produce CO gas, which was consistent with Masatoshi [25] and Brandstadt et al. [21]. Zhu et al. [26] studied the oxidation kinetics of ANP in CO_2 and obtained the activation energies of the two oxidation stages, which were 206.38 KJ/mol and 305.76 KJ/mol, respectively. In the study of reaction between ANP and H_2O, Saceleanu et al. [27] reported that two rate-determining stages existed in the micro/nano aluminum powder-liquid water system. These two stages were controlled by redox reactions and mass transport, respectively. Simulations by Russo et al. [28] demonstrated that the concentration of H_2O molecules had an important effect on the dissociation process of the ANP clusters.

In recent years, molecular dynamics (MD) simulations have been extensively performed to observe the behaviors of atoms during the oxidation process of ANP. However, most of the previous researches concentrate on the reaction of ANP with a single oxidant (O_2, CO_2, or H_2O) [10,24,28]. As far as we know, there are few systematic simulations on the ignition and combustion of ANP in a complex mixture environment. In this work, the ReaxFF molecular dynamics method was employed to simulate the heat transfer and gas-particle reaction of core–shell ANP under different hot pure/mixture atmospheres. The effects of oxidant components on the ignition delay time and reaction heat release of ANP were obtained. The results of this paper are expected to provide theoretical guidance for the control of ANPs ignition and combustion in complex environments.

2. Method

2.1. Reactive force field

The ReaxFF reactive force field is commonly used in molecular dynamics, and it is performed in the simulations of most elements in the periodic table [29–33]. The parameters of ReaxFF are derived from experimental results and the principles of quantum mechanics. ReaxFF reactive force field is based on a bond-order mechanism to describe the

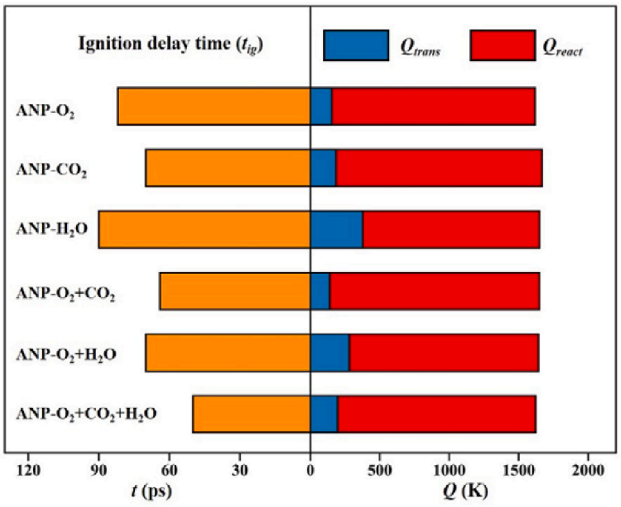

Fig. 2. Ignition delay time (left part) and contributions of heat transfer and reaction heat release before ignition (right part) in the six atmospheres.

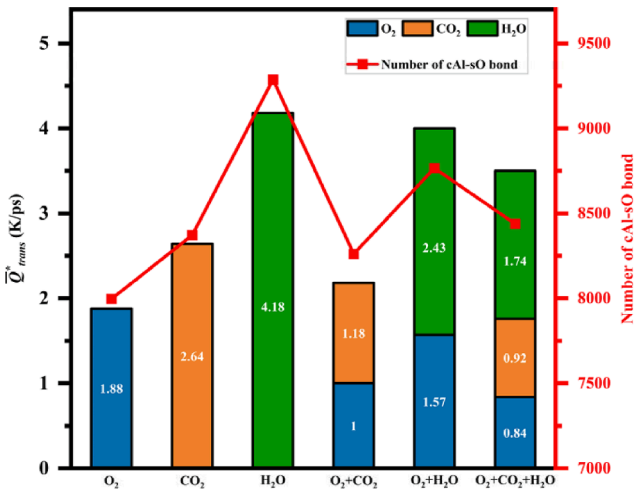

Fig. 3. Average heat transfer rate of oxidizers before ignition (the left axis) and the number of cAl-sO bond at ignition (the right axis) in the six atmospheres.

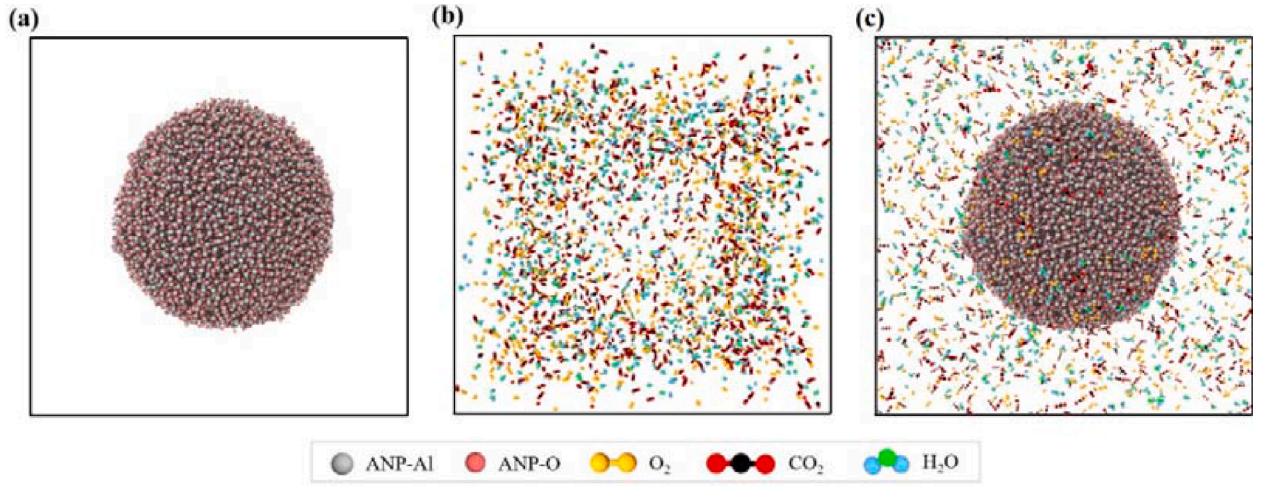

Fig. 1. Snapshots of models: (a) the core–shell ANP; (b) the oxidizers mixtures of O_2, CO_2, and H_2O; (c) the initial configuration of ANP surrounded by oxidizers.

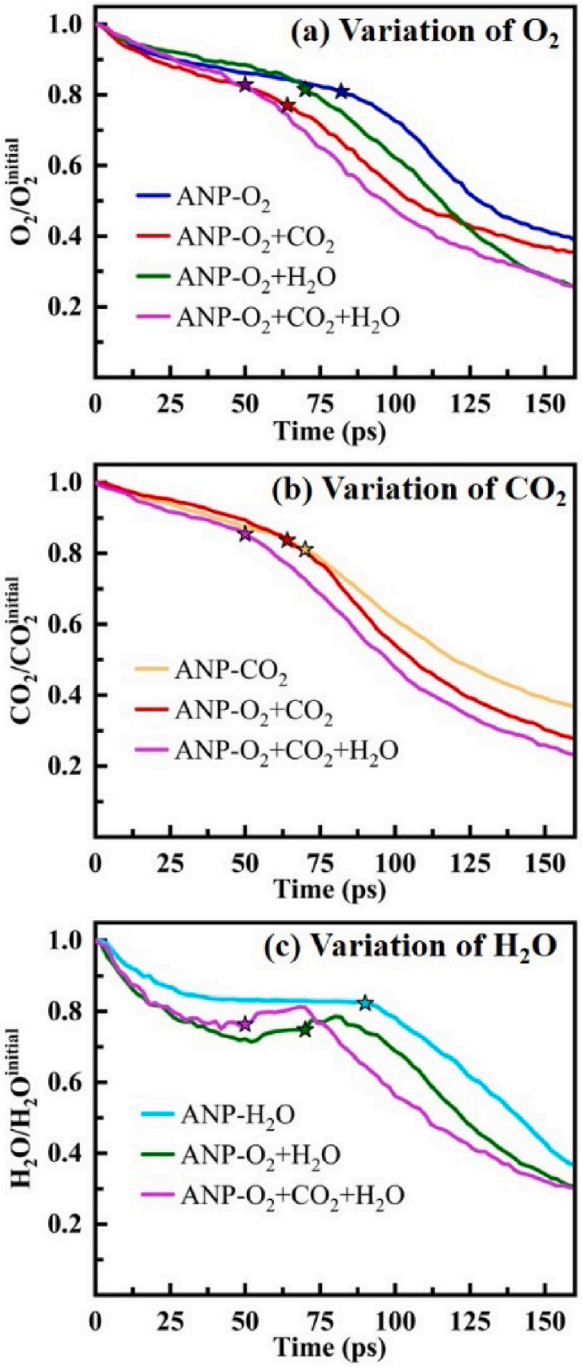

Fig. 4. Variation of (a) O_2, (b) CO_2, and (c) H_2O in six environments. The oxidizer concentrations are normalized by initial values. The star symbols represent ignition time.

formation and breaking of chemical bonds [34], and it is capable to compute the large-scale reactive systems (>1000 atoms), which is challenging to be described by DFT or nonreactive force fields. It has been proved that ReaxFF reactive force field can precisely characterize the microstructure of metal particles and it is suitable for simulating the physicochemical evolution of metal particles burning in oxidizers [35]. A systematic overview of the development, applications, and future directions of ReaxFF can be seen in reference [36] by Senftle et al. [36].

Bond-order between atom i and j (BO_{ij}) can be directly calculated from the distance r_{ij}. The computation method is given as

$$BO_{ij} = BO_{ij}^{\sigma} + BO_{ij}^{\pi} + BO_{ij}^{\pi\pi} = \exp[p_{bo1}(\frac{r_{ij}}{r_0^{\sigma}})^{p_{bo2}}] + \exp[p_{bo3}(\frac{r_{ij}}{r_0^{\pi}})^{p_{bo4}}] + \exp[p_{bo5}(\frac{r_{ij}}{r_0^{\pi\pi}})^{p_{bo6}}] \quad (1)$$

where p_{bo} terms are empirical parameters. r_0^{σ}, r_0^{π}, $r_0^{\pi\pi}$ are equilibrium bond lengths of σ, π and ππ bond character, respectively.

Due to the description of bond formation and breaking, the expression for total energy used in the ReaxFF is calculated by

$$E_{system} = E_{bond} + E_{over} + E_{under} + E_{lp} + E_{val} + E_{tors} + E_{vdWaals} + E_{Coulomb} \quad (2)$$

in which E_{system} is the total energy of the system. E_{bond}, E_{over}, E_{under}, E_{lp}, E_{val}, E_{tors} denote bond energy, overcoordination energy, undercoordination energy, lone pair energy, valence angle energy, and torsion angle energy, respectively. All of the above are bonding interactions energy, the van der Waals energy ($E_{vdWaals}$) and Coulomb energy ($E_{Coulomb}$) are nonbonded interactions energy, which are calculated separately.

The parameters of ReaxFF adopted in this paper can be found in the literature by Hong and van Duin et al. [37]. The same parameters were conducted by many other scholars to explore ANPs' ignition and combustion [38], aggregation and sintering [39], and ethanol oxidation over ANP [40].

2.2. Simulation details

To simulate the ANP combustion in different atmospheres, a core–shell structure ANP model with a diameter of 6 nm Al core and 1 nm thickness alumina shell was first constructed. The oxide shell of ANP was amorphous, which was formed by annealing the α-alumina. The number of core Al (cAl), shell Al (sAl), and shell O (sO) were 5388, 5778, and 8540, respectively. Then, the core–shell ANP relaxed for 160 ps under canonical ensemble (keep the number of atoms, volume, and temperature conserved, denoted as *NVT*) to obtain a more stable structure. The initial temperature of ANP was set as 300 K, and it was placed in the center of a 160◊160◊160 Å cubic box with periodic boundaries in all three directions. Moreover, a variety of typical oxidizers atmospheres models were established. Molecules in all atmospheres were randomly distributed, with a total number of 2700. All the oxidizers models were relaxed for 40 ps under *NVT* at 2000 K. The temperature of ANP and oxidizers were controlled by a Nose/Hoover thermostat. Finally, initial pre-oxidation systems were completed by combining the low-temperature core–shell ANP with the high-temperature oxidizers. The oxidation of ANP under different atmospheres was carried out in the microcanonical ensemble (keep the number of atoms, volume, and total energy conserved, denoted as *NVE*) with a timestep of 0.2 fs for 160 ps. This Non-Equilibrium Reactive Molecular Dynamics simulations were also employed by Rajabpour et al. to examine the heat transfer between a silver nanoparticle and surrounding water [41]. The timestep was proved to be suitable in references [15] and [39]. The temperature damping parameter was chosen to be 20 fs, 100 times of timestep. Detailed information on different systems is listed in Table 1. System ANP-O_2 means the ANP is surrounded by oxidizers consisting of O_2 and so on. No_2, Nco_2, and N_{H2O} represent the number of O_2, CO_2, and H_2O. Fig. 1 shows the ANP model, oxidizers model, and initial configuration ready for subsequent oxidation simulation in system ANP-O_2 + CO_2 + H_2O. All the molecular dynamics simulations and visualization in this paper were performed by LAMMPS [42,43] and OVITO [44], respectively.

3. Results and discussion

3.1. Heat transfer and reaction heat release before ignition

In the early oxidation stage, a lot of heat will be transferred to ANP due to the high gas temperature. In addition, accompanied by the re-

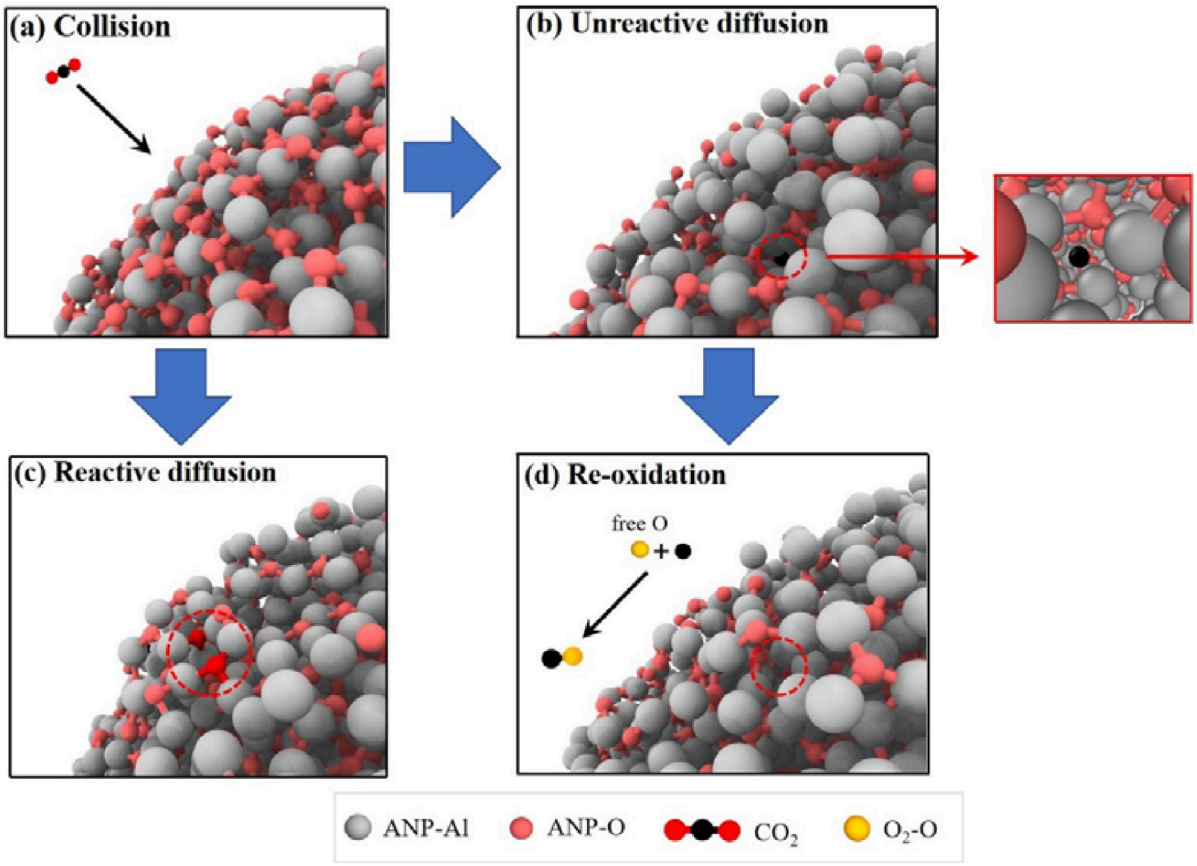

Fig. 5. Schematic diagram of (a) collision, (b) unreactive diffusion, (c) reactive diffusion, and (d) re-oxidation in system ANP-O_2 + CO_2.

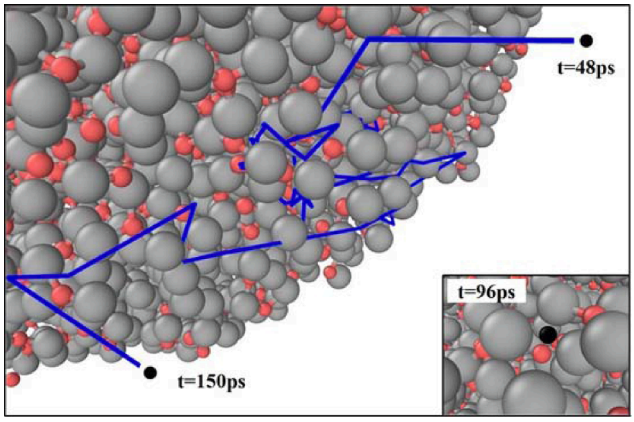

Fig. 6. Trajectory capturing the unreactive diffusion and detachment of C atom (grey, Al atom; red, O atom; black, C atom). (For interpretation of the references to colour in this figure legend, the reader is referred to the web version of this article.)

action between ANP and oxidizers, a large amount of reaction heat will be generated. Both the heat transfer (Q_{trans}) and reaction heat release (Q_{react}) will increase the temperature of ANP, resulting in ANP ignition (the moment of core Al atoms consumption rate reaches its maximum). Thus, the ignition delay time (t_{ig}), Q_{trans} and Q_{react} before ANP ignition in the six atmospheres were examined, and the results are shown in Fig. 2. The contribution of Q_{trans} and Q_{react} is calculated by [45]

$$Q = \frac{\Delta E}{3N_p k_B} \tag{3}$$

where N_P is the number of ANP atoms, and k_B is the Boltzman constant. ΔE represents the energy variation of the oxidizers kinetic and system potential energy in the calculations of Q_{trans} and Q_{react}.

It can be seen in Fig. 2 that t_{ig} of mixed oxidizers environments are shorter than that in pure oxidizers environments. For example, t_{ig} of system ANP-O_2 + CO_2 is smaller than that of system ANP-O_2 and system ANP-CO_2, as well as system ANP-O_2 + H_2O, ANP-O_2, and ANP-H_2O. And t_{ig} of system ANP-O_2 + CO_2 + H_2O is the shortest. Additionally, the right part of Fig. 2 shows that the total energy of ignition in different initial atmospheres is almost the same. It indicates that the ignition of ANP is independent on the oxidizers, which is consistent with the results of Chu et al. [24]. In the pure oxidizer systems (ANP-O_2, ANP-CO_2, and ANP-H_2O), heat transfer to ANP in the H_2O environment is much larger than that in the O_2 and CO_2. Even in the mixed oxidizers systems (ANP-O_2 + CO_2, ANP-O_2 + H_2O, and ANP-O_2 + CO_2 + H_2O), Q_{trans} increases when the oxidizing environment contains H_2O molecules. However, compared with heat transfer, reaction heat release plays a more significant role in particle's ignition. Though Q_{trans} of system ANP-H_2O is more than others, it experiences a long ignition delay time.

To further illustrate the heat transfer capacity of oxidizer molecules in the early stage of oxidation of ANP, the average heat transfer rate of different ambient gases (denoted as $\overline{Q}^{*}_{trans}$) before ignition was investigated. (Since the duration of heat transfer from gas to ANP before ignition is different in the six environments, $\overline{Q}^{*}_{trans}$ can better reflect the heat transfer capacity of different oxidizers.) As shown in Fig. 3, in the environment of three pure oxidizers, the relationship of heat transfer capacity can be expressed as $\overline{Q}^{H2O}_{trans} > \overline{Q}^{CO2}_{trans} > \overline{Q}^{O2}_{trans}$. In the mixed oxidizers, $\overline{Q}^{O2+H2O}_{trans} > \overline{Q}^{O2+CO2+H2O}_{trans} > \overline{Q}^{O2+CO2}_{trans}$. In addition, $\overline{Q}^{O2}_{trans}$, $\overline{Q}^{CO2}_{trans}$, and $\overline{Q}^{H2O}_{trans}$ in the mixed oxidizers still follow the relationship in the pure oxidizers. The red curve in Fig. 3 shows the number of cAl-sO bond at ignition, which can reflect the core–shell reaction to a certain extent. It can be

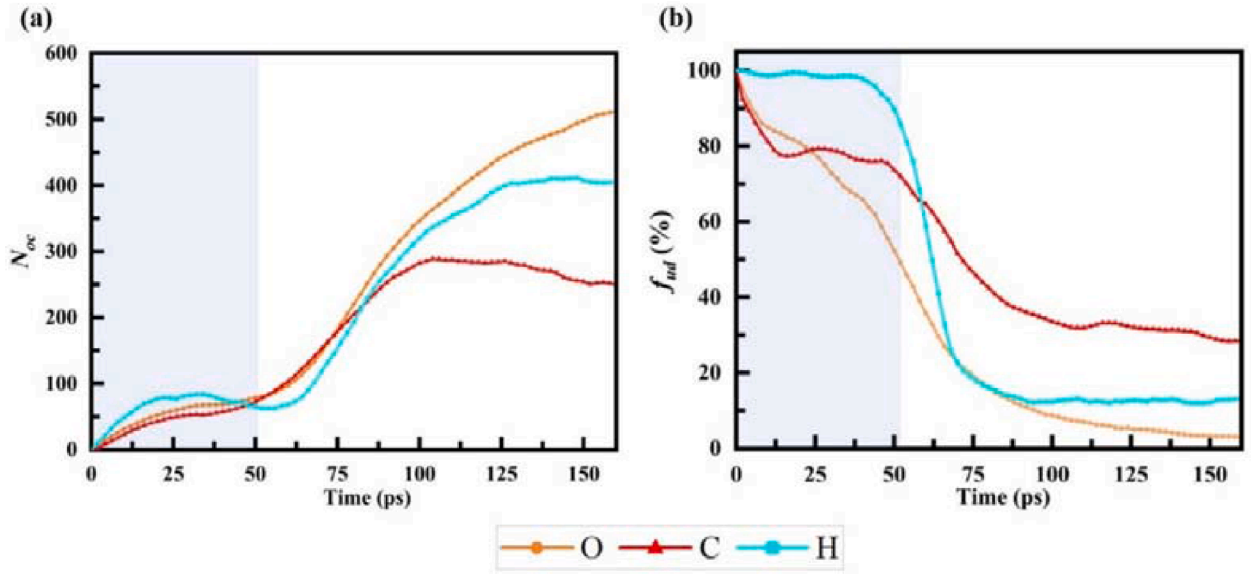

Fig. 7. (a)The number of oxidizer atoms collide into particle (N_{oc}), and (b) corresponding fraction of oxidizer atoms in unreactive diffusion in the system ANP-O_2 + CO_2 + H_2O. The shadow region represents the ignition stage.

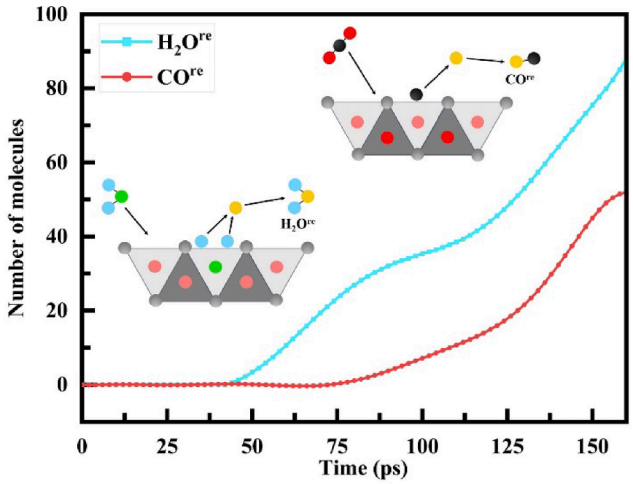

Fig. 8. Variations of H_2O^{re} and CO^{re} during the re-oxidation process in the system ANP-O_2 + CO_2 + H_2O. The illustrator shows the formation of H_2O^{re} and CO^{re} on ANP surface.

seen that the cAl-sO bond will be more in the atmosphere with a high average heat transfer rate. This is because the gas transfers more heat to the particle, causing the atoms in the particle move more violently. Then, the outward diffusion of cAl and the inward diffusion of sO are accelerated, and the cAl-sO bond will be created more easily.

3.2. Reaction mechanism between ANP and oxidizer mixtures

3.2.1. Number of oxidizer molecules

As mentioned in Section 3.1, the reaction heat release is the main factor in the ignition of ANP. In this section, the number of oxidizer molecules during the oxidation will be discussed. The variation of ambient gas molecules is plotted in Fig. 4. Normalization was performed due to the difference in the number of initial gas molecules ($O_2^{initial}$, $CO_2^{initial}$, and $H_2O^{initial}$) in the six environments. In Fig. 4 (a) and (b), O_2 and CO_2 are consumed lightly before ignition. After ignition, the consumption rate of the two increase rapidly with the acceleration of the reaction. In the mixed oxidizer environments, the consumption fraction of O_2 and CO_2 are larger than that in the pure oxidizer environments. Unlike O_2 and CO_2, the number of H_2O molecules (Fig. 4c) decrease quickly in the early stage. In the system ANP-H_2O, after a sharp drop, the number of H_2O molecules remain stable until ignition, indicating no extra H_2O participate in the ANP oxidation at this stage. However, in the system ANP-O_2 + H_2O and ANP-O_2 + CO_2 + H_2O, the number of H_2O increases slightly around ignition. It means that a few H_2O molecules are generated during this period. Then, just like O_2 and CO_2, H_2O molecules also undergo a process of rapid consumption. At the end of the simulation, it is also observed that the proportion of H_2O consumed in the mixed oxidizer environments are more significant than that in the pure H_2O environment. In short, compared with pure oxidizer atmospheres, the oxidation of ANP in mixed oxidizer atmospheres consume more gas molecules.

3.2.2. Reaction modes in oxidizer mixtures

The oxidation and combustion of ANP is the process of mutual diffusion between oxidizer atoms and particle atoms [15]. After diffusing into particle, a part of oxidizer atoms will bond with Al, while some will not. Taking the system ANP-O_2 + CO_2 as an example, Fig. 5 shows the three reaction modes oxidizer atoms involved in after colliding into particle. The CO_2 molecule slowly approaches ANP and collides with it. After the collision, the C—O bonds in the CO_2 molecule break. Then, C and O diffuse into ANP. The two O atoms are involved in reactive diffusion mode, bonding with Al atoms in the particle (Fig. 5c), while C atom does not (Fig. 5b). As the reaction proceeds, a new mode is observed: re-oxidation. If O_2 exists in the environment, the free O (from the O-O bond breaking in the environment O_2) slowly approaches ANP. At the same time, the nonbonded C detaches from the ANP and bonds with the free O, producing CO. Finally, the CO diffuses into the environment. The collision, unreactive diffusion and reactive diffusion in Fig. 5(a), (b) and (c) is the basic process of ANP combustion [24]. However, the re-oxidation in Fig. 5(d) only appears in the mixed oxidizer environments. It allows the oxidizer atoms, which do not bond with ANP atoms, to bond with the free gas atoms, and further increase the reaction heat release. The experimental results of aluminum particle combustion in different oxidizing environments [46] may be explained by this oxidation process.

Typical MD trajectory of C is captured as indicated in Fig. 6 to illustrate the unreactive diffusion and re-oxidation. The O atoms in the gas are not shown in Fig. 6. At 48 ps, C atom appears near the ANP. After

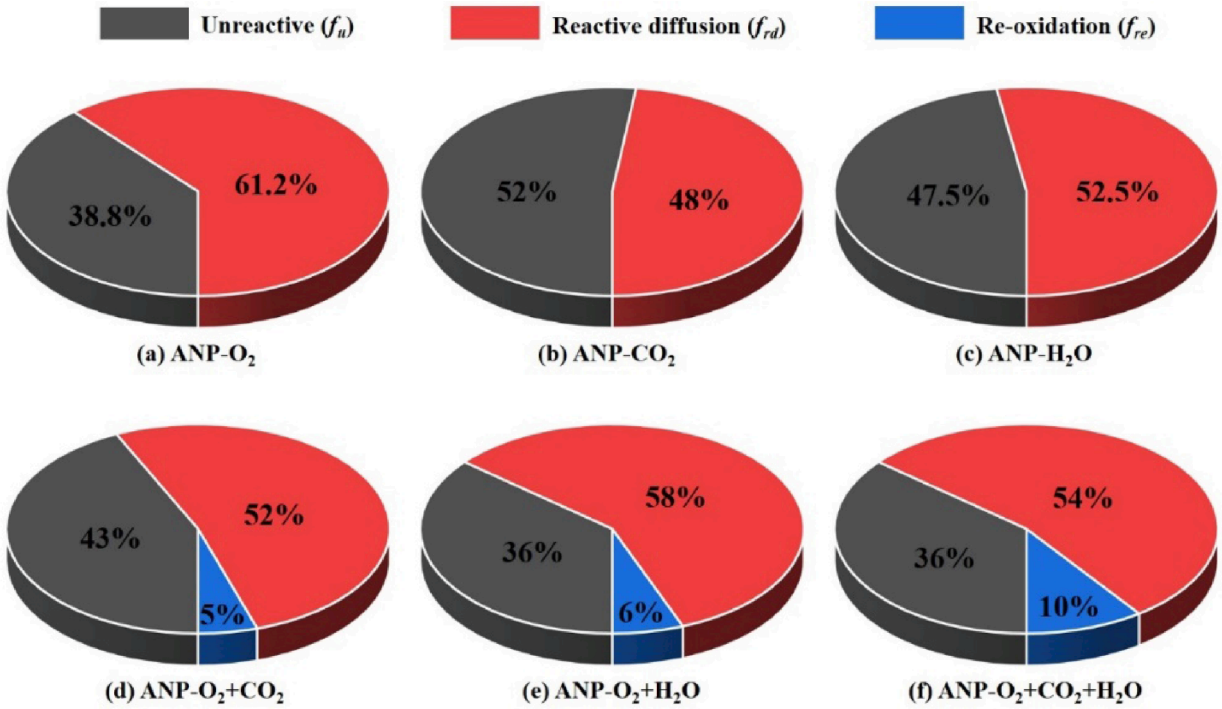

Fig. 9. Proportions of oxidizer atoms in unreactive, reactive diffusion, and re-oxidation at the end of the simulation in the six atmospheres.

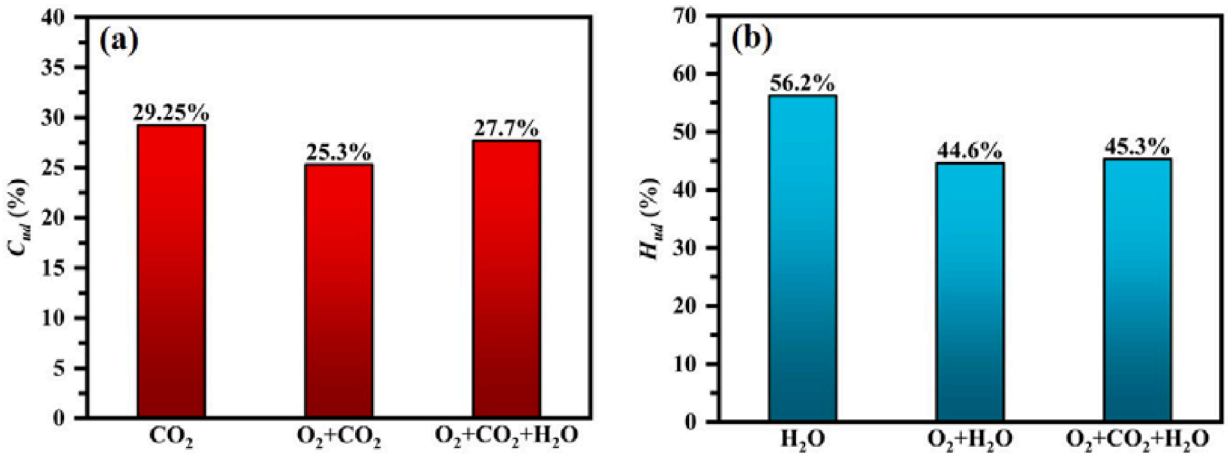

Fig. 10. Proportions of (a) C, (b) H atoms in unreactive diffusion at the end of simulation (t = 160 ps).

the collision of CO_2 molecule and ANP, the C atom diffuses into particle. The snapshot in the lower right shows the unreactive diffusion C at 96 ps. Then, the C atom moves to the surface of ANP and detaches. Finally, at 150 ps, it appears in the distance. In fact, C atom has been bonded with O atom in oxygen at this moment. But it should be noted that from 48 ps to 150 ps, the C atom does not bond with Al or O in the ANP.

Based on the analysis above, oxidizer atoms fall into two categories which collide into the particle or move in the environment. Moreover, oxidizer atoms collide into particles contain unreactive diffusion and reactive diffusion. The unreactive diffusion oxidizer atoms do not bond with particle atoms. These atoms occupy binding sites around Al and transfer a lot of heat to ANP. When there exists another oxidizer in the environment, these atoms may be re-oxidized. Owing to the energy release of bonds, the oxidizer atoms in reactive diffusion and re-oxidation are the key sources of reaction heat release.

Furthermore, taking system ANP-O_2 + CO_2 + H_2O as an example, the number of oxidizer atoms collide into particle and the fraction of unreactive diffusion (f_{ud}), defined as the ratio of the number of unreactive diffusion oxidizer atoms to the number of oxidizer atoms collide into particle (Eq (4)), are plotted in Fig. 7 to illustrate the behavior difference of C, H, and O atoms.

$$f_{ud} = \frac{N_{ud}}{N_{oc}} = \frac{N_{ud}}{N_{ud} + N_{rd}} \tag{4}$$

where N_{ud}, N_{rd}, and N_{oc} are the number of oxidizer atoms in unreactive diffusion, reactive diffusion, and collide into particle.

As seen in Fig. 7(a), H atoms collide into particle are the fastest at the initial stage of the reaction. These high-temperature H atoms transfer plenty of heat to ANP. Thus, the average heat transfer rate of H_2O in Fig. 3 is the largest. At the stage before ANP ignition (shadow in Fig. 7), the N_{oc} of H atoms rises rapidly and then falls, indicating that parts of H atoms break away from the particle and diffuse into the environment. Compared with H atoms, the N_{oc} of C atoms reaches a peak at about 100 ps, and it drops thereafter. This trend indicates that after 100 ps, the rate

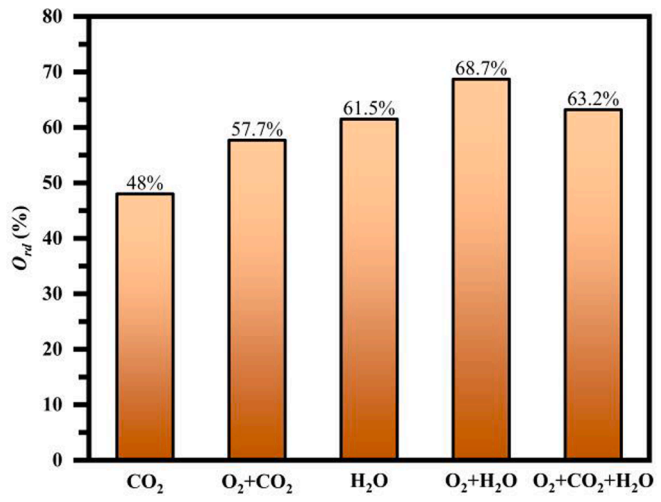

Fig. 11. Proportion of reactive diffusion for O atoms in the oxidizers at the end of the simulation (t = 160 ps).

of C atoms collide into particle is less than that diffuse outward to the environment. The N_{oc} of O atoms keeps increasing during the whole reaction. At the end of the simulation, the N_{oc} of O atoms is the most, which reaches 513, more than that of H and C, 405 and 252, respectively. Observing the curves in Fig. 7(b), the f_{ud} of H atoms is almost 100 % before ignition. It means that these H atoms hardly bond with Al before ignition. The f_{ud} of C atoms decreases slightly faster than O at the initial stage. But at the stage of 15–50 ps, it is relatively stable. The reason should be that with the accumulation of C atoms on the particle surface, the reaction of subsequent C atoms is hindered [24]. At this stage, the f_{ud} of O atoms shrinks rapidly, and exceeds that of C atoms. After the ignition of ANP, the f_{ud} of C, H, and O atoms drops fleetly. After 75 ps, the f_{ud} curve of H atoms does not decrease significantly, and the N_{oc} curve is still increasing. It illustrates that the reaction rate of H atoms tends to be stable. Likewise, after 100 ps, the f_{ud} of C atoms almost does not decrease, but the N_{oc} curve shows a small drop, indicating that C atoms mainly undergo re-oxidation reaction at this stage, a large amount of C atoms diffusing outward. As for O atoms, its f_{ud} is the lowest. Almost all the O atoms colliding into ANP are involved in reactive diffusion, bonding with Al.

The variations of H_2O and CO generated by re-oxidation (denoted as H_2O^{re} and CO^{re}) and the re-oxidation process in system ANP-O_2 + CO_2 + H_2O are shown in Fig. 8. After H_2O molecule collides into particle, the O atom bond with Al, while H atoms do not. At the stage of H atoms diffuse outward in Fig. 7(a), $H2O^{re}$ begin to appear, which means that re-oxidation occurs at this time. H atoms bond with free O in the environment and produce extra H_2O. This is why the number of H_2O in Fig. 4 (c) slightly increases. Similarly, the number of CO^{re} begins to rise at about 75 ps, indicating that parts of C atoms experience re-oxidation and produce CO.

3.2.3. Influences of re-oxidation

In mixed atmospheres, re-oxidation will influence the behavior of oxidizer atoms. The fraction of oxidizer atoms in unreactive (including moves in the environment and unreactive diffusion), reactive diffusion, and re-oxidation (denoted as f_u, f_{rd}, and f_{re}) in different environments are examined as shown in Fig. 9. They are calculated by

$$f_u = \frac{N_e + N_{ud}}{N_{total}} \tag{5}$$

$$f_{rd} = \frac{N_{rd}}{N_{total}} \tag{6}$$

$$f_{re} = \frac{N_{re}}{N_{total}} \tag{7}$$

where N_{total} is the total number of oxidizer atoms in different atmospheres. N_e, N_{ud}, N_{rd}, N_{re}, are the number of oxidizer atoms move in the environment, unreactive diffusion, reactive diffusion, and re-oxidation, respectively.

Based on the definition of reactive diffusion, it occurs between particle atoms and oxidizer atoms, which can reflect the oxidation degree of ANP. In Fig. 9, the lowest f_{rd} is the ANP-CO_2 system. Only 48 % of the 8,100 gas atoms participate in reactive diffusion. And the f_{rd} in system ANP-O_2 is the largest, indicating that the oxidation degree of ANP in O_2 environment is the highest. When adding O_2 in pure CO_2 or H_2O, the f_{rd} will increase lightly. Moreover, in mixed gas environments, the f_u significantly decreases due to the re-oxidation. In the system ANP-O_2 + CO_2, the f_u is only 43 %, which is 9 % lower than the system ANP-CO_2. And 5 % gas atoms are involved in re-oxidation. Similarly, in system ANP-O_2 + H_2O, the f_u is 11.5 % lower than that in system ANP-H_2O, and its f_{re} is 6 %. In the system ANP-O_2 + CO_2 + H_2O, the f_u is only 36 %, and the f_{re} even reaches 10 %. Notably, compared to system ANP-CO_2 and ANP-H_2O, the f_u in system ANP-O_2 + CO_2 and ANP-O_2 + H_2O decrease significantly. It is because that plenty of nonbonded C and H atoms detach from the ANP, causing other gas atoms diffusion into ANP and bond with Al, increasing the reaction heat release.

To explore the influence of re-oxidation on C and H atoms

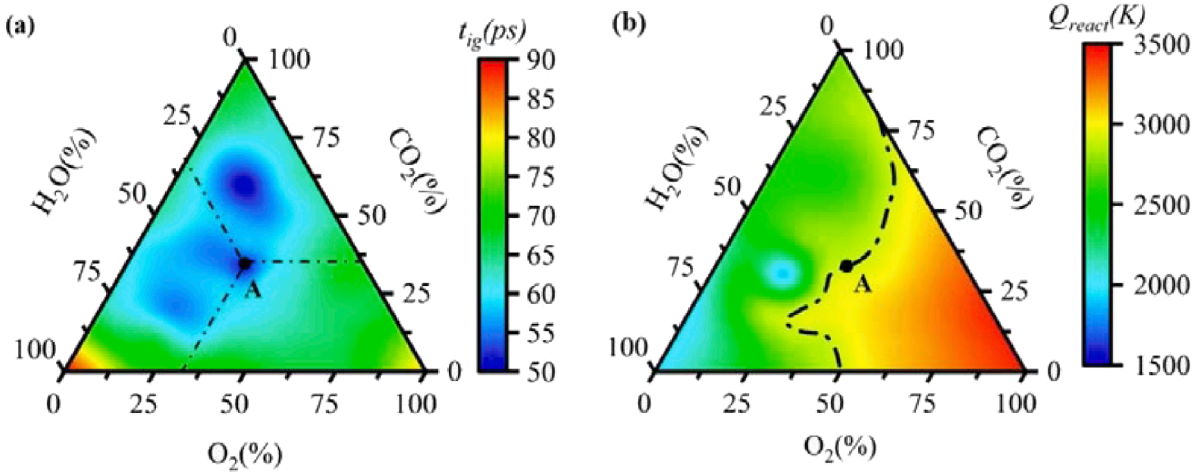

Fig. 12. (a) Ignition delay time and (b) reaction heat release in different atmospheres. Chain-dotted line in (a) is the coordinate of point A and (b) is the contour line of reaction heat release reaching 2900 K.

quantitatively, the fraction of C and H atoms involved in unreactive diffusion in different atmospheres (defined as the ratio of C or H atoms in unreactive diffusion to the total number of C or H atoms, denoted as C_{ud} and H_{ud}) are examined, as shown in Fig. 10. According to Fig. 10(a), in the three environments containing CO_2, C_{ud} in mixed oxidizers systems are 25.3 % and 27.7 %, slightly lower than that in system ANP-CO_2 (29.25 %). Fig. 10(b) shows that in the three environments containing H_2O, H_{ud} values in mixed oxidizer systems are notably lower than that in system ANP-H_2O. It indicates that re-oxidation reduces C and H atoms in unreactive diffusion inside the particle, releasing the binding site around Al atoms. And the reduction of H atoms is more significant than C atoms.

In addition, Fig. 11 shows the fraction of O atoms involved in reactive diffusion in different environments (defined as the ratio of O atoms in reactive diffusion to the total number of O atoms, denoted as O_{rd}). It can be seen that O_{rd} in system ANP-O_2 + CO_2 is larger than that in system ANP-CO_2. Similarly, O_{rd} in oxidizer mixtures of O_2 and H_2O is more significant than that in a pure H_2O environment. And the O_{rd} in oxidizer mixtures of O_2, CO_2, and H_2O is also more prominent than in a pure CO_2 or H_2O environment. The increasement of O_{rd} means that O atoms reoccupy the binding sites around the Al and bonding with Al atoms.

3.3. Optimize the ignition delay time and reaction heat release

The above analyses of heat transfer and reaction between oxidizer atoms and ANP are at the micro level. The specific effects of these phenomena on the macro mainly reflect the ignition delay time and reaction heat release of ANP. Therefore, the ignition delay time and reaction heat release of ANP in different environments are calculated. As shown in Fig. 12(a), ANP will experience a relatively long ignition delay time in an environment with more than 90 % O_2 or H_2O (lower left and lower right regions in Fig. 12(a)). In environments with more O_2, the heat transfer from gas to ANP is poor at the initial oxidation stage, resulting in a slow temperature rise of ANP. And in environments with more H_2O, the heat transfer rate is fast in the early stage, but H atoms diffusing into ANP do not bond with Al, leading to less reaction heat. The ignition delay time of ANP will be effectively reduced if the contents of CO_2 and H_2O in the range of 20 %–75 % and the content of O_2 in the range of 10 %–50 % (blue region in Fig. 12(a)). As for reaction heat release, the environment with more O_2 will relatively increase the reaction heat release, as shown in Fig. 12(b). When the concentration of CO_2 and H_2O in the atmosphere is high, the reaction heat release will be low. Briefly, by tailoring the contents of three oxidizers (O_2, CO_2, and H_2O) in the environment, the ignition delay time and reaction heat release can be adjusted to achieve the optimal performance of ANP combustion. For instance, the chain-dotted line in Fig. 12(b) represents the contour line of reaction heat release (Q_{react}) reaching 2900 K. Point A in Fig. 12(a) is the contents of oxidizers (n_{O_2} = 35 %, n_{CO_2}=32 %, n_{H_2O} = 33 %) with the shortest ignition delay time (50 ps) under the Q_{react} of 2900 K.

4. Conclusion

In this study, ReaxFF molecular dynamics simulations were performed to study the heat transfer and reaction heat release in the ignition and combustion process of ANP under O_2, CO_2, H_2O, and their mixture atmospheres. The ignition of ANP is triggered by heat transfer and reaction heat release, where the reaction heat release contributes more significantly. ANP experiences a shorter ignition delay time in mixed oxidizer atmospheres. The core–shell reaction of ANP is closely related to the average heat transfer rate of oxidizers. The number of cAl-sO bonds at ignition will increase in the atmosphere with a higher average heat transfer rate, resulting from the atoms in the particle move more violently. In the early stage of combustion, H_2O molecules transfer heat to ANP at the fastest rate due to the rapid diffusion of H atoms. Before ignition, H atoms almost do not bond with Al. C and O atoms diffuse slowly in the early stage, but they bond with Al easily after collision with ANP. Collision, unreactive diffusion, and reactive diffusion are the basic processes during ANP oxidation. While in the environment of mixed oxidizers, oxidizer atoms will be involved in a new reaction mode: re-oxidation. Re-oxidation of H atoms occurs around ANP ignition. Nonbonded H atoms inside the particle diffuse to the environment and bond with free O atoms in the environment to produce H_2O molecules, resulting in a temporary increase in the quantity of H_2O. Re-oxidation of C atoms occurs after 75 ps and produces additional CO. The re-oxidation reduces the number of C and H atoms in unreactive diffusion and increases the fraction of O atoms in reactive diffusion. In addition, re-oxidation also increases the fraction of oxidizer atoms bonding with Al. In conclusion, this work reveals that the ANP combustion characteristics (ignition delay time and reaction heat release) are largely determined by the contents of O_2, CO_2, and H_2O in the environment, which are expected to provide a theoretical guide for applying aluminum nanoparticles in various oxidizers.

CRediT authorship contribution statement

Yintao Zhou: Investigation, Writing – original draft. **Baolu Shi:** Methodology, Writing – review & editing. **Qingzhao Chu:** Visualization, Writing – review & editing. **Lijuan Liao:** Supervision, Writing – review & editing.

Declaration of Competing Interest

The authors declare that they have no known competing financial interests or personal relationships that could have appeared to influence the work reported in this paper.

Data availability

Data will be made available on request.

Acknowledgment

This work is supported by the National Natural Science Foundation of China (Grant U20B2018 and 52106130). QC acknowledges support from the State Key Laboratory of Explosion Science and Technology (Grant QNKT23-15) and the Beijing Institute of Technology Research Fund Program for Young Scholars.

References

[1] D. Sundaram, V. Yang, R.A. Yetter, Metal-based nanoenergetic materials: synthesis, properties, and applications, Prog. Energy Combust. Sci. 61 (2017) 293–365, https://doi.org/10.1016/j.pecs.2017.02.002.
[2] S. Gumus, H. Ozcan, M. Ozbey, B. Topaloglu, Aluminum oxide and copper oxide nanodiesel fuel properties and usage in a compression ignition engine, Fuel 163 (2016) 80–87, https://doi.org/10.1016/j.fuel.2015.09.048.
[3] T.R. Sippel, T.L. Pourpoint, S.F. Son, Combustion of nanoaluminum and water propellants: effect of equivalence ratio and safety/aging characterization, Propellants Explos. Pyrotech. 38 (2013) 56–66, https://doi.org/10.1002/prep.201200143.
[4] H.T. Huang, M.S. Zou, X.Y. Guo, R.J. Yang, Y.K. Li, Analysis of the aluminum reaction efficiency in a hydro-reactive fuel propellant used for a water ramjet, Combust. Explos. Shock Waves 49 (2013) 541–547, https://doi.org/10.1134/S0010508213050055.
[5] J.M. Bergthorson, Recyclable metal fuels for clean and compact zero-carbon power, Prog. Energy Combust. Sci. 68 (2018) 169–196, https://doi.org/10.1016/j.pecs.2018.05.001.
[6] C. Mandilas, G. Karagiannakis, A.G. Konstandopoulos, C. Beatrice, M. Lazzaro, G. Di Blasio, et al., Study of basic oxidation and combustion characteristics of aluminum nanoparticles under enginelike conditions, Energy Fuel 28 (2014) 3430–3441, https://doi.org/10.1021/ef5001369.
[7] P. Bucher, R.A. Yetter, F.L. Dryer, E.P. Vicenzi, T.P. Parr, D.M. Hanson-Parr, Condensed-phase species distributions about Al particles reacting in various oxidizers, Combust. Flame 117 (1999) 351–361, https://doi.org/10.1016/S0010-2180(98)00074-1.

[8] Y.S. Kwon, A.A. Gromov, A.P. Ilyin, E.M. Popenko, G.H. Rim, The mechanism of combustion of superfine aluminum powders, Combust. Flame 133 (2003) 385–391, https://doi.org/10.1016/S0010-2180(03)00024-5.
[9] W. Wang, R. Clark, A. Nakano, R.K. Kalia, P. Vashishta, Effects of oxide-shell structures on the dynamics of oxidation of Al nanoparticles, Appl. Phys. Lett. 96 (2010) 1–4, https://doi.org/10.1063/1.3425888.
[10] B. Wu, F.C. Wu, Y.B. Zhu, A.M. He, P. Wang, H.A. Wu, Fast reaction of aluminum nanoparticles promoted by oxide shell, J. Appl. Phys. (2019) 126, https://doi.org/10.1063/1.5115545.
[11] Y. Li, R.K. Kalia, A. Nakano, P. Vashishta, Size effect on the oxidation of aluminum nanoparticle: multimillion-atom reactive molecular dynamics simulations, J. Appl. Phys. (2013) 114, https://doi.org/10.1063/1.4823984.
[12] A. Rai, D. Lee, K. Park, M.R. Zachariah, Importance of phase change of aluminum in oxidation of aluminum nanoparticles, J. Phys. Chem. B 108 (2004) 14793–14795, https://doi.org/10.1021/jp0373402.
[13] Q. Chu, B. Shi, L. Liao, Y. Zhou, K.H. Luo, N. Wang, Size-derived reaction mechanism of core-shell aluminum nanoparticle, Appl. Phys. Lett. (2020) 117, https://doi.org/10.1063/5.0015367.
[14] T. Bazyn, H. Krier, N. Glumac, Combustion of nanoaluminum at elevated pressure and temperature behind reflected shock waves, Combust. Flame 145 (2006) 703–713, https://doi.org/10.1016/j.combustflame.2005.12.017.
[15] Q. Chu, B. Shi, L. Liao, K.H. Luo, N. Wang, C. Huang, Ignition and oxidation of core-shell Al/Al 2 O 3 nanoparticles in an oxygen atmosphere: insights from molecular dynamics simulation, J. Phys. Chem. C 122 (2018) 29620–29627, https://doi.org/10.1021/acs.jpcc.8b09858.
[16] A. Rai, K. Park, L. Zhou, M.R. Zachariah, Understanding the mechanism of aluminium nanoparticle oxidation, Combust. Theory Model. 10 (2006) 843–859, https://doi.org/10.1080/13647830600800686.
[17] X. Zou, N. Wang, L. Liao, Q. Chu, B. Shi, Prediction of nano/micro aluminum particles ignition in oxygen atmosphere, Fuel 266 (2020), 116952, https://doi.org/10.1016/j.fuel.2019.116952.
[18] X. Zhang, C. Fu, Y. Xia, Y. Duan, Y. Li, Z. Wang, et al., Atomistic origin of the complex morphological evolution of aluminum nanoparticles during oxidation: a chain-like oxide nucleation and growth mechanism, ACS Nano 13 (2019) 3005–3014, https://doi.org/10.1021/acsnano.8b07633.
[19] G. Li, L. Niu, W. Hao, Y. Liu, C. Zhang, Atomistic insight into the microexplosion-accelerated oxidation process of molten aluminum nanoparticles, Combust. Flame 214 (2020) 238–250, https://doi.org/10.1016/j.combustflame.2019.12.027.
[20] Y. Tang, C. Kong, Y. Zong, S. Li, J. Zhuo, Q. Yao, Combustion of aluminum nanoparticle agglomerates: from mild oxidation to microexplosion, Proc. Combust. Inst. 36 (2017) 2325–2332, https://doi.org/10.1016/j.proci.2016.06.144.
[21] K. Brandstadt, D.L. Frost, J.A. Kozinski, Preignition characteristics of nano-and micrometer-scale aluminum particles in Al-CO2 oxidation systems, Proc. Combust. Inst. (2009) 32, https://doi.org/10.1016/j.proci.2008.08.014.
[22] W. Yang, W. Shi, C. Chen, T. Zhang, J. Liu, Z. Wang, et al., Efficiency analysis of a novel electricity and heat co-generation system in the basis of aluminum–water reaction, Int. J. Hydrogen Energy 42 (2017) 3598–3604, https://doi.org/10.1016/j.ijhydene.2016.08.207.
[23] S. Mercati, M. Milani, L. Montorsi, F. Paltrinieri, Design of the steam generator in an energy conversion system based on the aluminum combustion with water, Appl. Energy 97 (2012) 686–694, https://doi.org/10.1016/j.apenergy.2012.01.028.
[24] Q. Chu, B. Shi, L. Liao, X. Zou, K.H. Luo, N. Wang, Reaction mechanism of the aluminum nanoparticle: physicochemical reaction and heat/mass transfer, J. Phys. Chem. C 124 (2020) 3886–3894, https://doi.org/10.1021/acs.jpcc.9b11410.
[25] M. Saba, T. Kato, T. Oguchi, Chemical kinetics modeling for combustion of Al in CO_2, Combust. Flame 233 (2021), 111613, https://doi.org/10.1016/j.combustflame.2021.111613.
[26] B. Zhu, T. Du, Y. Sun, Oxidation kinetics of nano-aluminum in a carbon dioxide environment, Prog. React. Kinet. Mech. 41 (2016) 14–22, https://doi.org/10.3184/146867816X14525972784045.
[27] F. Saceleanu, T.V. Vuong, E.R. Master, J.Z. Wen, Tunable kinetics of nanoaluminum and microaluminum powders reacting with water to produce hydrogen, Int. J. Energy Res. 43 (2019) 7384–7396, https://doi.org/10.1002/er.4769.
[28] M.F. Russo, R. Li, M. Mench, A.C.T. Van Duin, Molecular dynamic simulation of aluminum-water reactions using the ReaxFF reactive force field, Int. J. Hydrogen Energy 36 (2011) 5828–5835, https://doi.org/10.1016/j.ijhydene.2011.02.035.
[29] M. Zheng, X. Li, J. Liu, L. Guo, Initial chemical reaction simulation of coal pyrolysis via ReaxFF molecular dynamics, Energy Fuel 27 (2013) 2942–2951, https://doi.org/10.1021/ef400143z.
[30] K. Chenoweth, A.C.T. van Duin, A. William, I. Goddard, ReaxFF reactive force field for molecular dynamics simulations of hydrocarbon oxidation, Chem. A Eur. J. 112 (2008) 1040–1053.
[31] S. Huygh, A. Bogaerts, A.C.T. Van Duin, E.C. Neyts, Development of a ReaxFF reactive force field for titanium dioxide/water systems, Comput. Mater. Sci. 95 (2014) 579–591, https://doi.org/10.1016/j.commatsci.2014.07.056.
[32] S. Hong, A. Krishnamoorthy, P. Rajak, S. Tiwari, M. Misawa, F. Shimojo, et al., Computational synthesis of MoS2 layers by reactive molecular dynamics simulations: initial sulfidation of MoO3 surfaces, Nano Lett. 17 (2017) 4866–4872, https://doi.org/10.1021/acs.nanolett.7b01727.
[33] A.C.T. Van Duin, A. Strachan, S. Stewman, Q. Zhang, X. Xu, W.A. Goddard, ReaxFFSiO reactive force field for silicon and silicon oxide systems, Chem. A Eur. J. 107 (2003) 3803–3811, https://doi.org/10.1021/jp0276303.
[34] A.C.T. Van Duin, S. Dasgupta, F. Lorant, W.A. Goddard, ReaxFF: a reactive force field for hydrocarbons, Chem. A Eur. J. 105 (2001) 9396–9409, https://doi.org/10.1021/jp004368u.
[35] S. Hong, A.C.T. Van Duin, Molecular dynamics simulations of the oxidation of aluminum nanoparticles using the ReaxFF reactive force field, J. Phys. Chem. C 119 (2015) 17876–17886, https://doi.org/10.1021/acs.jpcc.5b04650.
[36] T.P. Senftle, S. Hong, M.M. Islam, S.B. Kylasa, Y. Zheng, Y.K. Shin, et al., The ReaxFF reactive force-field: development, applications and future directions, npj Comput. Mater. 2 (2016), https://doi.org/10.1038/npjcompumats.2015.11.
[37] S. Hong, A.C.T. Van Duin, Atomistic-scale analysis of carbon coating and its effect on the oxidation of aluminum nanoparticles by ReaxFF-molecular dynamics simulations, J. Phys. Chem. C 120 (2016) 9464–9474, https://doi.org/10.1021/acs.jpcc.6b00786.
[38] P. Liu, J. Liu, M. Wang, Ignition and combustion of nano-sized aluminum particles: A reactive molecular dynamics study, Combust. Flame 201 (2019) 276–289, https://doi.org/10.1016/j.combustflame.2018.12.033.
[39] Y. Cheng, Y. Zhao, F. Zhao, S. Xu, X. Ju, C. Ye, ReaxFF simulations on the combustion of Al and n- butanol nanofluid, Fuel 330 (2022), https://doi.org/10.1016/j.fuel.2022.125465.
[40] Y.R. Zhang, A.C.T. van Duin, K.H. Luo, Investigation of ethanol oxidation over aluminum nanoparticle using ReaxFF molecular dynamics simulation, Fuel 234 (2018) 94–100, https://doi.org/10.1016/j.fuel.2018.06.119.
[41] A. Rajabpour, R. Seif, S. Arabha, M.M. Heyhat, S. Merabia, A. Hassanali, Thermal transport at a nanoparticle-water interface: A molecular dynamics and continuum modeling study, J. Chem. Phys. 150 (2019), https://doi.org/10.1063/1.5084234.
[42] A.P. Thompson, H.M. Aktulga, R. Berger, D.S. Bolintineanu, W.M. Brown, P. S. Crozier, et al., LAMMPS - a flexible simulation tool for particle-based materials modeling at the atomic, meso, and continuum scales, Comput. Phys. Commun. 271 (2022), 108171, https://doi.org/10.1016/j.cpc.2021.108171.
[43] H.M. Aktulga, J.C. Fogarty, S.A. Pandit, A.Y. Grama, Parallel reactive molecular dynamics: Numerical methods and algorithmic techniques, Parallel Comput. 38 (2012) 245–259, https://doi.org/10.1016/j.parco.2011.08.005.
[44] A. Stukowski, Visualization and analysis of atomistic simulation data with OVITO-the Open Visualization Tool, Model. Simul. Mater. Sci. Eng. 18 (2010), https://doi.org/10.1088/0965-0393/18/1/015012.
[45] Q. Chu, X. Chang, D. Chen, A physiochemical model for the combustion of aluminum nano-agglomerates in high-speed flows, Combust. Flame 237 (2022), 111739, https://doi.org/10.1016/j.combustflame.2021.111739.
[46] F. Halter, V. Glasziou, M. Di Lorenzo, S. Gallier, C. Chauveau, Peculiarities of aluminum particle combustion in steam, Proc. Combust. Inst. (2022) 1–10, https://doi.org/10.1016/j.proci.2022.07.120.